

# MICRO INERTIAL REFERENCE SYSTEM FOR MICROSPACECRAFT

Tony K. Tang, Roman C. Gutierrez, Christopher B. Stell,  
Vatche Vorperian, Kirill Shcheglov, Linda M. Miller,  
Judith A. Podosek, William J. Kaiser\*

Jet Propulsion Laboratory  
MicroDevices Laboratory, California Institute of Technology  
4800 Oak Grove, Pasadena, CA 91109-8099

\*Department of Electrical Engineering,  
University of California, Los Angeles, CA 90024-1594

## ABSTRACT

This paper reports on the development of a silicon bulk micromachined vibratory gyroscope designed for a micro inertial reference system for microspacecraft applications. This silicon vibratory microgyroscope design consists of a four leaf clover silicon structure with a central post suspended by four thin silicon cantilevers. This device is electrostatically actuated at one of its fundamental modes, and input rotation is detected by monitoring the Coriolis induced motions of the leaves capacitively. The bias stability of this microgyroscope is typically 30 deg/hr with angle random walk of  $<1.5$  deg/ $\sqrt{\text{hr}}$ , and scale factor nonlinearity of  $<1\%$ . This device has a small temperature dependent frequency shift of 0.23 Hz/degree for both the drive and sense modes. The microgyroscope and its pre-amplifier electronics are housed inside a hermetically sealed package approximately  $1 \times 1 \times 1.5 \text{ cm}^3$  in size. The rest of the control electronics which includes the oscillator and lock-in amplifier circuitry and A/D converter are mounted outside the gyro box on a 6.4 cm x 8.9 cm circuit board. This new vibratory microgyroscope offers potential advantages of long operational life, high performance, extremely compact size, low power operation, and low cost.

## INTRODUCTION

Future space exploration missions will require microspacecraft that are 10 to 1000 times lower in cost, mass, volume, and power consumption than present generations of spacecraft such as the Galileo and the Cassini spacecraft (Figure 1). These drastic reductions lead to similar changes in the navigation, guidance, and attitude control systems of the spacecraft. Present navigation, guidance, and attitude control systems that use conventional gyroscope technologies are exceedingly costly, massive, and consume too much power for microspacecraft applications.

Micromachined vibratory gyroscopes [1-5] are promising candidates to replace conventional gyroscopes in a new micro Inertial Reference System ( $\mu\text{IRS}$ ) for microspacecraft navigation, guidance, and attitude control applications (Figure 2). This  $\mu\text{IRS}$  will be used for attitude and maneuver control, and stabilization and pointing of instruments such as cameras, antenna, detectors, and solar panels. The  $\mu\text{IRS}$  can also supplement other external inertial reference sys-

tems[6] such as the Global Positioning System (GPS), sun sensor, or star tracker by "filling in the gaps" during times the direct use of these systems is not possible.

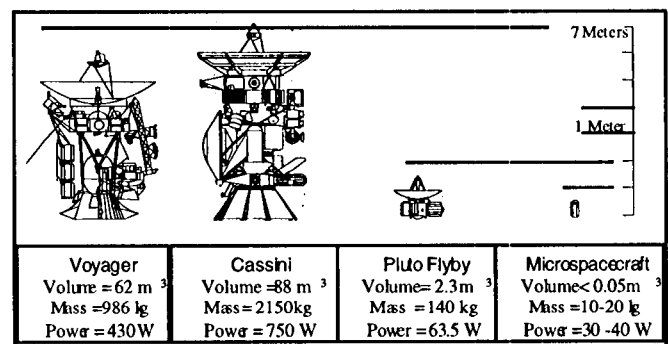


Figure 1. Comparison of microspacecraft with previous generation of large spacecraft.

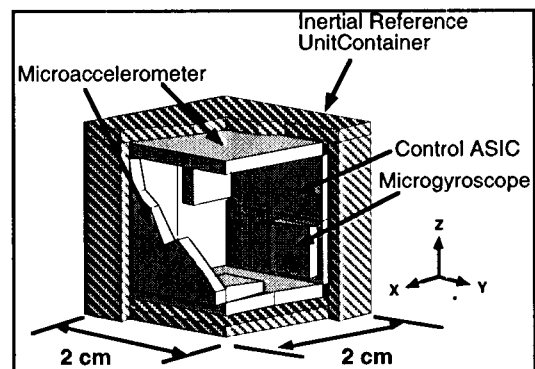


Figure 2. Schematic representation of a micro Inertial Reference System comprised of micromachined silicon microgyroscopes and microaccelerometers.

In this paper, we report on recent developments of a silicon bulk micromachined vibratory gyroscope which is a central component of the micro inertial reference system. This silicon vibratory microgyroscope is fabricated using simple, precise, and low-cost bulk silicon machining technology. The unique symmetric resonator design results in a highly sensitive design with degenerate drive and sense modes. The device is a very low loss resonator with high quality (Q) factor for mechanical amplification.

## DESCRIPTION

This silicon microgyroscope consists of a four leaf clover suspended by four thin wires with a post rigidly attached to the center in the direction perpendicular to the plane of the clover leaves (Figure 3). The rim, the clover structure and the suspensions are made from single crystal silicon. The silicon clover-leaf structure with the post is bonded to a silicon base plate patterned with gold electrodes. The clover leaves provide large areas for electrostatic drive and sensing. The four suspensions provide mechanical support and restoring force for the harmonic motion of the whole structure. The post provides a large Coriolis force coupling between the orthogonal modes when the gyroscope rotates about the post axis. The mechanical resonant frequencies of the microgyroscope vary according to design in the 300 to 2000 Hz range. The three lowest order mechanical modes are 1) up/down mode in which all the leaves move along the z-axis simultaneously, 2) rocking mode about the y-axis, and 3) rocking mode about the x-axis. One of these rocking modes functions as the "drive" mode and the other orthogonal rocking mode is the "sense" mode.

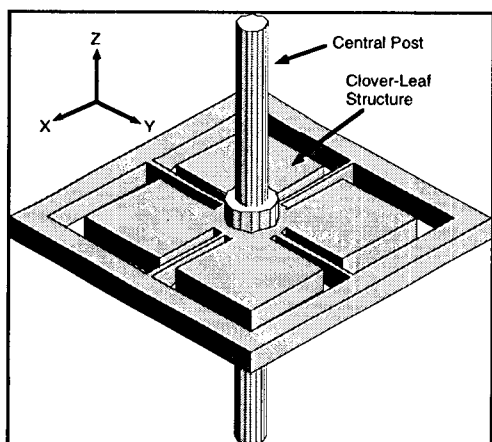


Figure 3. Schematic drawing of the microgyro structure.

The clover-leaf structure is electrostatically driven to oscillate at the "drive" mode, rocking about one of the in-plane axes (i.e. y-axis). Since the post is rigidly attached to the clover-leaf structure, the post follows the same motion. Under rotation, Coriolis acceleration induces energy transfer from the "drive" mode to the "sense" mode causing the post to rock about the x-axis (in addition to its motion about the y-axis). The motion of the post is translated back into the rocking motion of the clover leaves. The post provides a large Coriolis coupling which transfers energy between the two orthogonal rocking modes.

The highest rotation sensitivity is obtained when the drive and sense modes have the same resonant frequency. Very stringent fabrication and assembly requirements are necessary to achieve this "matched" condition. When this "matched" condition is achieved, the response to the Coriolis

acceleration is then amplified by the Q factor of the resonance resulting in improved sensor performance and reduced drive voltage. The two rocking modes of the clover-leaf structure are symmetrical in the x-y plane and are inherently degenerate.

## FABRICATION

The clover-leaf microgyroscope design consists of three major components: the silicon clover-leaf structure, the silicon baseplate, and the vertical post. The fabrication steps of the silicon clover-leaf structure and the baseplate are similar, involving two masking and etching steps and one metallization step. The starting material for both the clover-leaf structure and the baseplate are <100> silicon double-side polished wafers with two epilayers grown on top. The buried epilayer is 4 microns thick doped with Boron ( $10^{20}/\text{cm}^3$ ) and counter-doped with 2% Ge for stress relief. The top silicon epilayer is 26 microns thick doped with Phosphorous.

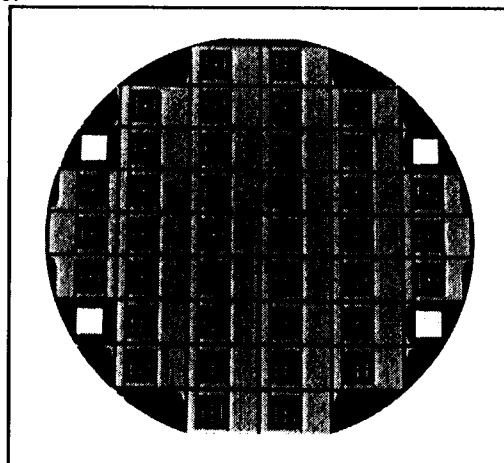


Figure 4. Clover-leaf structures on a 4-in. Si wafer.

The fabrication procedure for the clover-leaf structure begins with the deposition of a thin layer (1000Å) of LPCVD  $\text{Si}_3\text{N}_4$  onto the silicon wafer. This  $\text{Si}_3\text{N}_4$  layer is patterned with the clover leaf pattern and used as a mask for ethylene diamine pyrocatechol (EDP) etching of the 26 microns silicon epilayer to the p+ etch-stop layer. After the EDP etch, the thin  $\text{Si}_3\text{N}_4$  mask is removed and another 1000Å thick  $\text{Si}_3\text{N}_4$  is grown on the entire wafer. This  $\text{Si}_3\text{N}_4$  layer on the wafer backside is also patterned and etched. Cr/Pt/Au is then e-beam evaporated onto the clover leaf structure and patterned. Then the whole wafer is again etched in EDP to remove the silicon substrate up to the p+ etch-stop layer (Figure 4). Next, the wafer is cleaved into individual devices and reactive ion etched with  $\text{SF}_6$  and  $\text{O}_2$  until the p+ stop-etch layer is removed. Finally, the remaining  $\text{Si}_3\text{N}_4$  layer is removed using a  $\text{CF}_4/\text{O}_2$  plasma.

The fabrication process of the silicon baseplate is similar to that used for the fabrication of the clover-leaf structure but with an additional oxidation step before the metallization step. After the first EDP etch, a low temperature silicon di-

oxide and an LPCVD  $\text{Si}_3\text{N}_4$  layer are grown onto the whole wafer. The topside  $\text{Si}_3\text{N}_4$  and oxide layer are patterned and etched to provide electrical contact to the p+ stop etch layer. The backside  $\text{Si}_3\text{N}_4$  and oxide layer are also patterned and etched. Metallization consisting of Cr/Pt/Au is then e-beam evaporated onto the silicon wafer and patterned. The entire wafer is then etched in EDP to remove the silicon substrate and to provide a hole for the placement of the post.

The clover-leaf structure and the baseplate are bonded together using a low temperature thermocompression bonding method. In this process, gold metallization on the clover leaf structure and the baseplate are heated to 300-600°C in vacuum. Then pressure is applied to the entire structure for several hours to bond the components together. During this bonding process, gold diffusion is enhanced by the application of heat and pressure, and results in a metal bond. This bond is very strong; the silicon structures usually shatter before the bond fails. The total bond line is < 4000 Å thick and uniform (Figure 5).



Figure 5. Bonded components using low temperature gold thermocompression bonding. The inserted SEM picture shows the gold bond line between two silicon wafers.

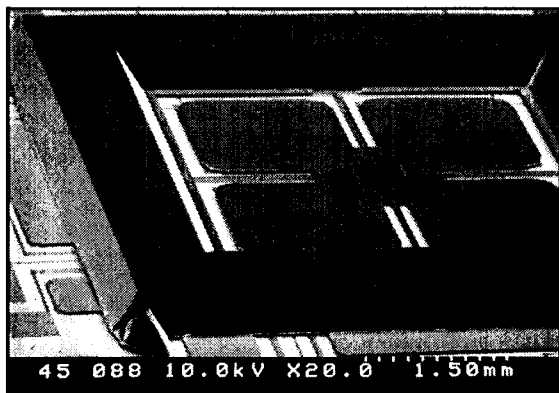


Figure 6. SEM picture of bonded clover-leaf structure with silicon baseplate before the assembly of the central post.

The bonded devices (Figure 6) are first tested for resonant frequencies and mode shapes. After these initial tests, a metal or silicon post is epoxied into the hole on the silicon

resonator. The dimensions of the silicon clover-leaf structure is 7 mm x 7 mm, the dimensions of each clover leaf is 2 mm x 2 mm, and the post is 500 microns in diameter and 5 mm in length. The silicon base plate is 1.5 cm x 1 cm and is approximately 400 microns thick. The silicon baseplate consists of metallized pads for the bonding of the electronics directly onto the microgyroscope.

## CONTROL AND READOUT ELECTRONICS

The actuation, or drive, circuit is realized by designing an oscillator ( $H(s)$ ) around the microgyroscope which locks onto the drive resonance mode as shown in Figure 7. The purpose of summing the signals from both sense plates is to remove the differential signal between them and hence the response of the sense resonance is obtained from the feedback loop. The sense circuit, on the other hand, subtracts the signals from both sense plates in order to remove the common-mode drive signal. A lock-in amplifier is used to detect a differential signal induced due to rotation.

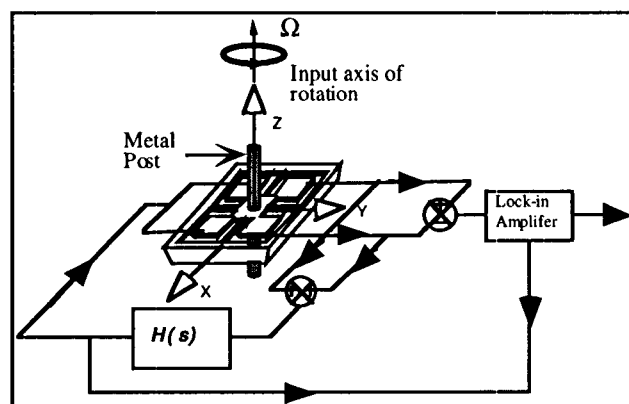


Figure 7. Block diagram of the microgyro control electronics.

## MEASUREMENT

The mechanical characteristics of the microgyroscopes are first identified in a custom test station which consists of a small vacuum chamber with electrical probes to electrically excite the microgyroscope, and a Polytech OFV 501 laser vibrometer (Doppler velocimeter) to accurately measure mechanical motion. This system is used to measure the resonance frequencies, Q-factors, mode shapes, hysteresis, snap-down voltage, symmetry (by exciting different electrodes), operational voltage, and survivability (by driving it with a very large amplitude signal) of the microgyroscope. The rotation testing of the microgyroscope uses a Triotech S347B rate table with a resolution of 0.01 degrees per second to rotate a micro-gyroscope inside a vacuum chamber, and a computer to record the output of the gyroscope as a function of rotation rate. The motion of the microgyroscope is measured both electrically and with a Polytech OFV 501 laser vibrometer.

The silicon microgyroscopes tested to date have mechanical resonant frequencies ~700 Hz, with a frequency split of <1%. The Q-factor of the drive and sense modes is typically

1000. Both resonant modes are rocking modes with nodal lines along the spring directions. The separation between the resonant frequencies is primarily due to thickness variations between the silicon suspensions and stress due to the bonding of the post to the clover leaf structure. Due to the close proximity of the "drive" and "sense" resonant frequencies, the response of this device is amplified by  $Q$ . However, since the  $Q$  of this device is relatively low, closed-loop feedback control electronics are not necessary to detect rotation rate. Presently, a single loop is used to control the motion of the microgyroscope because it is assumed that the device is perfectly fabricated. We have repeatably shown that, for our bulk micromachined gyroscope, the quadrature error is small in magnitude compared to the Coriolis signals we are measuring. The quadrature error may be further minimized by the addition of a second control loop to ensure that the microgyroscope is vibrating correctly.

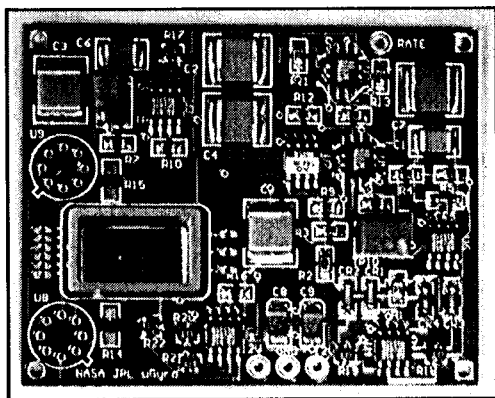


Figure 8. Packaged microgyro with control electronics.

The response of the microgyroscope to rotation rates is taken between  $-2$  deg/sec and  $+2$  deg/sec at room temperature. The driving voltage of the microgyroscope is approximately 100 mV peak to peak. The typical measured responsivity (scale factor) of the gyroscope is 200 mV/(deg/sec) with a scale factor nonlinearity of  $<1\%$  at an integration time of 1 second. Three consecutive tests are done to check for hysteresis and scale factor stability. Typical scale factor stability is 0.1% under ambient conditions with no hysteresis. The Green chart, which plots the two-sampled standard deviation (square root of the Allan variance) as a function of the integration time, is used to characterize the noise. Obtained values for angle random walk noise and bias stability are consistently  $< 1.5$  deg/ $\sqrt{\text{hr}}$  and  $< 30$  deg/hr, respectively. The present generation of microgyroscopes uses a silicon baseplate and a silicon vibrating structure resulting in small temperature dependent frequency variation of 0.23 Hz/degree for both the drive and sense modes.

## CONCLUSION AND FUTURE PLAN

This paper reports on recent experimental results on a new generation of silicon clover leaf microgyroscope designed for micro inertial reference system for microspacecraft applications. These new microgyroscopes have consistently

demonstrated a bias stability of  $< 30$  deg/hr, and a rate random walk of  $< 2$  deg/ $\sqrt{\text{hr}}$  with open-loop electronics and no temperature compensation. This clover-leaf microgyroscope is an avionics experiment on NASA's next generation space shuttle demonstrator X-33. This experiment consists of three packaged microgyroscopes to provide three-axes rotation detection. Each microgyroscope is individually packaged in a  $1.0 \times 1.0 \times 1.5$  cm<sup>3</sup> Kovar case (Figure 8).

In conclusion, the clover-leaf vibratory microgyroscope offers potential advantages of long operational life, high performance, extremely compact size, low power operation, and low cost for applications in inertial navigation and attitude control of microspacecraft. Continual improvement and optimization of the clover leaf microgyroscope will result in performance of less than 1deg/hr bias stability in the near future.

## ACKNOWLEDGMENTS

The work described in this paper was performed by the Center for Space Microelectronics Technology, Jet Propulsion Laboratory, California Institute of Technology, under contract with the National Aeronautics and Space Administration.

## REFERENCE

- 1 M. W. Putty, and K. Najafi, Tech. Digest, Solid-State Sensor & Actuator Workshop, Hilton Head Isl., SC, pp. 213-220, June 1994.
- 2 J. Bernstein, S. Cho, A. T. King, A. Kourepenis, P. Maciel, M. Weinberg, Digest, IEEE/ASME MEMS Workshop, Ft. Lauderdale, FL, pp. 143-148, February 1993.
- 3 P. Lung, T. Juneau, and A. Pisano, Proceedings of the ASME Dynamic Systems and Control Division, DSC-Vol. 57-2, 1995 IMECE/ASME, pp. 957-962.
- 4 T. Tang, R. Gutierrez, J. Wilcox, C. Stell, V. Vorperian, R. Calvet, W. Li, I. Chakraborty, R. Bartman, W. Kaiser, Tech Digest, Solid-State Sensor & Actuator Workshop, Hilton Head Isl., S.C. pp. 288-293, June 1996.
- 5 T. Tang, R. Gutierrez, C. Stell, V. Vorperian, G. Arakaki, J. Rice, W. Li, I. Chakraborty, K. Shcheglov, J. Wilcox, W. Kaiser, Digest, IEEE/ASME MEMS Workshop, Nagoya Castle, Japan, January 1997.
- 6 G. Sevaston, L. Craymer, & W. Breckenridge, 19th AAS Guidance & Control Conference, Breckenridge, CO, AAS 96-16, pp. 1-20. Feb. 7-11, 1996